Carlson, K.D., and Beckermann, C., "Sensitivity of Steel Casting Simulation Results to Alloy Property Datasets," in Proceedings of the 66th SFSA Technical and Operating Conference, Paper No. 5.3, Steel Founders' Society of America, Chicago, IL, 2012.

Sensitivity of Steel Casting Simulation Results to Alloy Property Datasets

Kent D. Carlson and Christoph Beckermann[1]

Department of Mechanical and Industrial Engineering

The University of Iowa, Iowa City, IA 52242

Abstract

The benchmark simulation Niyama results from the SFSA/MTI simulation qualification procedure are compared, and it is seen that the Niyama results for all benchmark alloys can be categorized into three groups, with each group being reasonably represented by a single alloy from that group: all nine steels (WCB, C5, C12, CA15, CD3MN, CD4MCuN, CF8M, CN3MN and CN7M) can be represented by the benchmark WCB dataset; Ni-based alloys N3M, CW6MC and CW12MW can be represented by the benchmark CW12MW dataset; and Ni-based alloys M30C and M35-1 can be represented by the benchmark M35-1 dataset. While these alloy groupings are applicable to the Niyama simulation qualification results, care must be taken in trying to generalize these groupings to other casting simulation results, because such grouping neglects property variation effects. The effects of four property variations are studied here: (1) solidification shrinkage; (2) liquidus temperature (superheat); (3) solidification path and latent heat; and (4) alloy composition, with respect to compositional variations within the specification range for an alloy. It is shown that differences in solidification shrinkage among alloys can lead to differences in both riser pipes and porosity indications within the casting. For a given pouring temperature, sizeable differences in liquidus temperatures among the benchmark alloys result in corresponding sizeable differences in pouring superheat, and such differences in superheat are shown to significantly impact the Niyama results. An example comparing simulation results from two different WCB datasets illustrates that variations in the solidification path and latent heat can result in significant differences in Niyama results. Finally, variation of composition within the specification range is studied for C12, and is seen to have a moderate effect on the Niyama results, but little effect on the resulting riser pipe prediction. The compositional ranges studied here are very broad, ranging effectively from the minimum to the maximum amount of alloying elements within the specification. While this broad composition variation does produce moderate changes in the Niyama results, it is expected that reasonable variations in chemistry would likely have little impact on the Niyama results. As a final caveat regarding the effect of property variations, note that only the Niyama and porosity results are investigated in this work. The effects of property variations on other simulation results, such as hot tears, has not been investigated.

[1] Author to whom correspondence should be addressed. Telephone: (319) 335-5681, Fax: (319) 335-5669, E-mail: becker@engineering.uiowa.edu

1. Introduction

For casting simulation results to truly reflect reality, accurate alloy material datasets (which specify thermophysical properties and the solid fraction-temperature relationship) must be utilized. This idea was one of the driving forces behind a recent collaborative effort between the SFSA, the MTI, and the University of Iowa, in which accurate material datasets were generated for a number of alloys of interest (referred to here as 'benchmark datasets' or 'benchmark alloys'), and a simulation qualification procedure was developed whereby simulation users can "validate" their simulation Niyama results for alloys included in the project by comparing them to Niyama results generated using the benchmark datasets[1]. The Niyama criterion is a local thermal parameter computed by casting simulation packages that is used to predict solidification shrinkage porosity. The simulation qualification project is explained in detail in Ref. [1]. The procedure used to produce the benchmark datasets is discussed in Ref. [2]. The benchmark datasets are available to SFSA members for download from the website: http://www.sfsa.org/folio/downloads/datasets/

In discussions regarding the accuracy of alloy properties, the following question has often been asked, but has yet to be truly investigated: How much of a difference do variations in alloy property data make in simulation results? This broad question encompasses many aspects that directly affect foundry simulation users. How important is it to have an accurate solid fraction-temperature curve[2] and latent heat value? Can a simulation user get reasonable results for one steel grade using an accurate material dataset from another steel grade? If a user has an accurate dataset for a particular steel grade, does that dataset still give realistic results when the composition is varied within the specification of that grade? The present study investigates questions such as these, and attempts to give casting simulation users a general sense of the impact that property variations can have on simulation results.

In Section 2, properties from the benchmark datasets are compared. The benchmark simulation results for these alloys are then compared and grouped based on Niyama and riser pipe results in Section 3. The suggested groupings are of interest in terms of the qualification simulation, but caution must be used in trying to generalize these groupings, because property variations can have a significant impact on simulation results. The importance of property variations on simulation results is investigated in Section 4.

2. Alloy Dataset Comparison

Before looking at simulation results, it is informative to compare properties among the benchmark alloys. There are currently fourteen alloy datasets included in the simulation qualification project. There are nine steel grades (C5, C12, CA15, CD3MN, CD4MCuN, CF8M,

[2] While the solid fraction-temperature curve (referred to here as the solidification path) and solidification range are technically not properties because they depend on the cooling rate, the term 'properties' will be extended to include them in this paper, for simplicity.

CN3MN, CN7M, WCB) and five nickel-based alloys (CW6MC, CW12MW, M30C, M35-1, N3M).

The solidification paths for these benchmark alloys are shown together in Fig. 1. As expected, the paths for the nickel-based alloys (dashed lines) have lower temperature ranges than those for the steels (solid lines). Note that although some of the solidification paths have kinks in them (indicating the formation of new solid phases) while others do not, these curves do have some common features. The slope of the solidification paths are generally very steep near liquidus (i.e., solid fraction = 0), and often rather shallow at the end of solidification, as the solid fraction approaches unity. The liquidus temperatures are compared in Fig. 2. The steels have liquidus values ranging from about 1380°C (2516°F) to 1500°C (2732°F), with the liquidus generally decreasing as the nickel content increases. The nickel-based alloys have liquidus values ranging from about 1300°C (2372°F) to 1375°C (2507°F). The solidification (freezing) ranges are compared in Fig. 3. The steel alloys have freezing ranges between about 70°C (126°F) and 110°C (198°F), while the nickel-based alloys have somewhat broader freezing ranges between about 110°C (198°F) and 150°C (270°F).

The latent heat values for the benchmark alloys are given in Fig. 4. The steel values range from 150 to 210 kJ/kg, and the nickel-based values have a similar range from about 160 to 230 kJ/kg. While some of these values may seem a bit low, they are comparable to values from thermodynamic simulation software packages, and the use of these values in simulations of casting experiments yielded excellent agreement between simulated and measured metal temperature values during solidification[1-2].

The thermal diffusivities of the benchmark alloys (evaluated at solidus[3]) are compared in Fig. 5. Thermal diffusivity, α, is defined as the ratio $\alpha = k/\rho c_p$, where k is the thermal conductivity, ρ is the density and c_p is the specific heat. Note that the thermal diffusivity of all steels, as well as CW6MC and CW12MW, are essentially the same. The thermal diffusivity of N3M is higher because N3M contains about 30% molybdenum, and the diffusivities of M30C and M35-1 are higher still because they contain 26 – 36% copper.

Finally, Fig. 6 compares the solidification shrinkage values for the benchmark alloys. The solidification shrinkage, β, is defined as: $\beta = (\rho_{sol} - \rho_{liq})/\rho_{liq}$, where ρ_{sol} and ρ_{liq} are the solidus and liquidus density values, respectively. The steel shrinkage values range from about 2.4% to 4.4%, while the nickel-based alloy values have a higher range of 4.3% to 6.8%.

3. Comparison of Simulation Qualification Benchmark Results

The casting geometry utilized in the simulation qualification procedure is the simple valve shown schematically in Fig. 7. This section contains the simulation results for all benchmark alloys. Simulations were performed using the casting simulation software MAGMAsoft[3], following the simulation qualification procedure (see Ref. [1] for details). Simulations were

[3] The term 'solidus' is used in this paper as shorthand notation to indicate the (non-equilibrium solidus) temperature at which an alloy becomes fully solid upon cooling.

performed for solidification-only (i.e., no filling), with a superheat of 100°C (180°F), where the superheat is defined as the difference between the initial simulation temperature and the liquidus temperature of the alloy being simulated. The sand was modeled as resin-bonded silica sand (using the FURAN database in MAGMA), with an initial temperature of 20°C (68°F). The interfacial heat transfer coefficient between the metal and the mold was taken as a constant value of 800 W/m^2-K. The riser was assumed to have hot topping (default MAGMA open riser boundary condition). The Niyama criterion evaluation temperature was taken to be 10% of the solidification range above the solidus temperature.

The Niyama results for the benchmark steel alloys are shown in Fig. 8, where the plane of the valve shown in these results is defined in Fig. 7(c). From Fig. 8, it is evident that the Niyama results for all steels look similar. There are certainly some differences: the size of the low-Niyama region in the middle of each result varies from alloy to alloy, and the distribution of the higher Niyama values seen in the left and right low-Niyama regions in each result (i.e., $0.7 < Ny < 1.4$ (°C-s)$^{1/2}$/mm) varies as well. However, the minimum Niyama value for all steel alloys is the same (i.e., $0 < Ny < 0.1$ (°C-s)$^{1/2}$/mm), and overall each result is similar. It should be noted that the differences mentioned above in the higher Niyama values in the left and right low-Niyama regions could be important in certain applications. For example, previous studies by the present authors[4-5] found that microporosity sufficient to cause leaks in fluid-containing castings may occur when a path from the inside to the outside of the casting exists where $Ny < 1 - 2$ (°C-s)$^{1/2}$/mm. With this in mind, one could compare the results in Fig. 8 for C5 and CN7M, for example, and realize that the CN7M casting is more likely to leak than the C5 casting.

Fig. 9 contains the Niyama results for the benchmark nickel-based alloys. There appear to be two distinct patterns of Niyama contours for these alloys. Alloys N3M, CW6MC and CW12MW all have similar contours, with left and right low-Niyama regions similar to the steels, and a middle low-Niyama region that is connected to the left low-Niyama region. Alloys M30C and M35-1 also have similar contours, with low-Niyama regions extending throughout most of the valve cross-section shown. The diffuse nature of the Niyama contours for M30C and M35-1 is due to the high copper content (and thus high thermal diffusivity) of these alloys.

Although the simulation qualification procedure only looks at the Niyama results shown in Figs. 8 and 9, it is also interesting to look at the porosity results for these simulations, in order to compare the riser pipes. Fig. 10 shows the cross-section of the valve used to view the riser pipes. Fig. 11 shows the riser pipes for the steel alloys. A reference line is included to compare the depth of the pipes. For all steel alloys, the riser pipe depths are similar. The shape of the riser pipes varies somewhat, however, due to the differences in the solidification shrinkage among these alloys seen in Fig. 6. The riser pipes for the nickel-based alloys are shown in Fig. 12. As with the steels, the riser pipe depths are similar, and the riser pipe shapes vary somewhat due to differences in solidification shrinkage.

Based on the results in Figs. 8-9 and 11-12, the benchmark alloys can be categorized into three groups, and a representative alloy can be selected from each group. The benchmark valve

simulation results from this representative alloy are indicative of the group the alloy represents, in terms of Niyama contours and the riser pipe. The steels are all included in one group, and represented by the benchmark WCB dataset. The nickel-based alloys are represented by two different groups: Group 1 (N3M, CW6MC and CW12MW) is represented by the benchmark CW12MW dataset, and Group 2 (M30C and M35-1) is represented by the benchmark M35-1 dataset.

4. Importance of Property Variations

The observations made in the previous section regarding the grouping of the benchmark alloys and the use of representative alloys for the simulation qualification results might lead one to conclude that the representative datasets for each group could be used in place of the actual alloys in any casting simulation, and reasonable simulation results could be expected. Such a generalization would be ill-advised, because it neglects important property variation effects. Four such property variations are investigated in this section: (1) solidification shrinkage; (2) liquidus temperature (superheat); (3) solidification path and latent heat; and (4) alloy composition, with respect to compositional variations within the specification range for an alloy.

All simulations performed for the studies in this section were performed as solidification-only. The sand mold in all simulations was simulated using MAGMA's FURAN dataset with an initial temperature of 20°C (68°F), and the interfacial heat transfer coefficient between the metal and the mold was taken as a constant value of 800 W/m^2-K. All simulations were performed with an initial metal temperature selected to give a 30°C (54°F) superheat, except the simulations in Section 4.2, where the effect of superheat is studied.

4.1 Solidification Shrinkage Effect

The first property variation of interest is solidification shrinkage. It is clear from Fig. 6 that there is considerable variation in the amount of solidification shrinkage among both the steels and the nickel-based alloys. In order to determine the effect this variation can have on simulation results, solidification of the simple casting shown in Fig. 13(a) was simulated. The casting has a hot spot at the end opposite the riser that the riser will not be able to feed. While this may not be a realistic example of a production casting, it does clearly illustrate the effect that variation in solidification shrinkage can have on simulation results.

Simulations for the casting shown in Fig. 13(a) were performed for four different alloys: steels CN3MN (β = 2.37%), CF8M (β = 3.55%) and WCB (β = 4.35%), and nickel-based alloy N3M (β = 5.73%). The simulated porosity results at the casting mid-plane are provided in Fig. 13(b). A dashed reference line is included at the bottom of the risers. Even though these castings were all simulated with the same superheat, the depth and shape of the riser pipe for each alloy differs, as does the size of the hole in the hot spot. These differences are primarily due to the differences in solidification shrinkage among these alloys. Obviously, the differences in riser pipe depth indicate that variations in solidification shrinkage can change the riser height required to obtain the desired safety margin. Also, by noting the difference in the size of the hot spot holes

between CN3MN and WCB, one can imagine that if the size of the hot spot region of the casting was reduced (e.g., by reducing the height of that region to less than the current 3.5 in.), a situation could be found where there was a significant porosity indication for WCB, but not for CN3MN. Thus, a difference in solidification shrinkage could mean the difference between predicting a hole and not predicting a hole.

4.2 Liquidus Temperature (Superheat) Effect

Figs. 1 and 2 clearly illustrate that there is a significant range of liquidus temperatures among both the steels and the nickel-based alloys being considered. This can be important if a simulation user is utilizing a representative alloy from the groups presented in Section 3, rather than using the actual alloy. Consider an example in which a simulation user wants to simulate a CN3MN casting using the benchmark WCB steel dataset. The user knows that the foundry typically pours this casting at 1530°C (2786°F), and inputs this value into the simulation. This creates a significant discrepancy in the alloy superheat: for CN3MN, this pouring temperature gives a superheat of 143°C (257°F), but for WCB, the superheat is only 28°C (50°F). So the simulated superheat is significantly smaller than the actual superheat.

To investigate the effect that such differences in superheat have on the simulation results, solidification of the 1 in. thick plate casting depicted in Fig. 14(a) was simulated for WCB, CF8M, CN3MN and N3M. In all simulations, the same initial temperature of 1530°C (2786°F) was specified, which results in the following superheats: 28°C (50°F) for WCB; 100°C (180°F) for CF8M; 143°C (257°F) for CN3MN; and 156°C (281°F) for N3M.

The Niyama results at the plate mid-thickness for this study are compared in Fig. 14(b). The dashed circle indicates the location of the riser in each casting. This comparison clearly illustrates that the size of the low-Niyama region decreases significantly as the superheat increases, which implies that higher superheats result in less shrinkage porosity. This is consistent with previous research by the present authors that correlated increases in the superheat to increases in riser feeding distances[6]. Note that the differences seen in the Niyama results in Fig. 14 are not related to solidification shrinkage; the Niyama criterion is a purely thermal criterion, which does not account for solidification shrinkage.

The riser pipes from these plate simulations are compared in Fig. 15. Note that the shapes and depths of the riser pipes vary from alloy to alloy. This effect is at least partially due to differences in the solidification shrinkage among these alloys, as described in Section 4.1. But superheat does account for some of the riser pipe shrinkage, because different superheats will produce different amounts of pure liquid shrinkage above the liquidus temperature. This can be seen in Fig. 15 by comparing the height of metal remaining in the riser pipes. For WCB, the metal on the sides of the riser pipe (i.e., blue regions of 0% porosity) reaches essentially all the way to the top of the riser. As the superheat increases, the height of metal at the sides of the riser lowers. For N3M, the highest metal in the riser is significantly lower than the top of the riser. The highest metal remaining in the riser indicates how far the liquid metal level in the riser

dropped before solidification began in that region, and this drop is seen to increase with superheat in Fig. 15.

4.3 Freezing Range and Latent Heat Effect

Next, an example of variations in the freezing range and latent heat is considered, by comparing simulation results from two different WCB datasets. The first dataset is the benchmark WCB dataset that has been utilized thus far in this work. The second dataset is the commonly-used MAGMA carbon steel dataset C19Mn5 (0.19% C, 1.25% Mn, 0.4% Si, 0.045% P, 0.045% S). The freezing ranges, latent heats and solidification shrinkages for these two datasets are compared in Table 1, and their solidification paths are compared in Fig. 16. Note in Table 1 that they have nearly the same liquidus temperature, but very different freezing ranges: C19Mn5 has a 39°C (70°F) freezing range, while the benchmark WCB dataset has a 91°C (164°F) range. Fig. 16 shows that the solidification paths for these two datasets are very similar for about the first 10°C (18°F) below liquidus, and then they are quite different. Another large discrepancy between the two datasets is the latent heat value. The benchmark WCB dataset uses a latent heat of 180 kJ/kg, while C19Mn5 uses 274 kJ/kg. Finally, note that even though the freezing ranges are very different, the solidification shrinkage values are similar. Since the liquidus and solidification shrinkage values for these two WCB datasets are similar, differences in the results can be attributed primarily to differences in the solidification paths and latent heats.

These datasets are compared using solidification simulation results for the 1 in. thick plate casting depicted in Fig. 14(a). The Niyama contours are compared in Fig. 17, and the riser pipes are compared in Fig. 18. The Niyama results for C19Mn5 in Fig. 17 show a significantly larger low Niyama region than the benchmark WCB dataset result, indicating that C19Mn5 gives a very conservative result (since lower Niyama values imply more shrinkage porosity). Note that the region where $Ny < 0.1$ $(°C\text{-}s)^{1/2}/mm$ for C19Mn5 is about the same size as the $Ny < 1.0$ region for the benchmark WCB. The riser pipes in Fig. 18 are similar, which is mainly due to the similarity in the solidification shrinkage between these two datasets, as discussed in Section 4.1, and the fact that the simulations used the same superheat, as discussed in Section 4.2.

4.4 Effect of Compositional Variations Within an Alloy Specification

The final property variation study investigates the effects on simulation results of compositional variations, within the allowable compositional ranges for an alloy specification. This is done by considering three compositions within the specification for C12. Table 2 shows the specified ranges for C12 alloying elements, along with three compositions. The composition labeled ‘actual’ is a measured composition from thermocouple casting experiments that were used to develop property datasets for C5, C12 and CA15—this work was an extension of the work described in Refs. [1-2]. The composition labeled ‘low’ uses weight percentages of the elements C, Mn, Si, Cr, Mo and Ni that are on the low end of the specified range: the minimum value was used if a minimum was specified for that element; otherwise, half of the maximum value was used. Similarly, the ‘high’ composition uses the maximum value of the specified ranges for the same elements mentioned above. The weight percentages of Ni, Cu, P and S were

not varied; rather, they were set equal to the 'actual' composition values. Note that the 'actual' composition falls nicely between the 'low' and 'high' compositions, providing three compositions that cover the C12 specification ranges.

The C12 specification was selected for this study because the thermodynamic simulation software used to generate the initial property datasets (IDS[7-8]) did a particularly good job with C12 in the development of the datasets mentioned above. The procedure used to develop property datasets for steels begins with an initial property dataset generated by IDS, given measured composition data and cooling rates during solidification as input. Corresponding experimental thermocouple data is then used to modify these IDS datasets until simulated thermocouple results are in good agreement with measurements (see Refs. [1-2] for details). In the case of C12 (using the 'actual' composition listed in Table 2), the IDS dataset gave good agreement with the measured thermocouple data. This is shown in Fig. 19, which compares a C12 thermocouple measurement to the corresponding prediction from the simulation using the initial (un-modified) IDS dataset. The measured solidus and liquidus values for C12 are compared to the un-modified IDS values in Table 3, again showing good agreement. Un-modified IDS datasets were used in this comparison because no experimental data was available to modify the datasets for the 'low' and 'high' compositions. C12 was selected because the un-modified IDS dataset gave good agreement for the 'actual' composition, thus implying that a comparison using un-modified IDS datasets for all three compositions would be realistic.

The solidification paths for the 'low', 'actual' and 'high' composition datasets are compared in Fig. 20, and the liquidus, solidus and solidification shrinkage values are compared in Table 4. The curves in Fig. 20 show that the liquidus temperature for C12 decreases as the alloying content increases, and that the freezing range increases as the alloying content increases. These observations are also reflected in Table 4, which also shows that the solidification shrinkage increases as the alloying content increases.

The three C12 datasets are compared using solidification simulation results for the 1 in. thick plate casting depicted in Fig. 14(a). The Niyama contours are compared in Fig. 21, and the riser pipes are compared in Fig. 22. The Niyama results in Fig. 21 show some difference in Niyama distributions: the low-Niyama region is largest for the 'low' composition and smallest for the 'high' composition. The 'actual' result is similar to the 'high' result, indicating a lower tendency toward shrinkage porosity than with the 'low' composition. The riser pipes compared in Fig. 22 for these three compositions are similar, due to similar solidification shrinkage values among the compositions and the fact that the same superheat was used in each simulation.

In summary, compositional variations were seen to produce some difference in Niyama results and little difference in riser pipe results over the C12 specification range. Considering that the compositional ranges investigated here varied from a minimum composition to a maximum composition, however, one would expect that reasonable variations in chemistry seen in day-to-day foundry practice would have little impact on the Niyama results produced by an accurate dataset for a particular alloy.

5. Conclusions

The material property datasets for the steel and nickel-based alloys included in the SFSA/MTI simulation qualification procedure (i.e., benchmark datasets) were compared, illustrating differences and similarities in the solidification paths, liquidus temperatures, solidification ranges, latent heat values, thermal diffusivities and solidification ranges. The benchmark Niyama simulation qualification results for these alloys were then categorized into three groups, with each group being reasonably represented by a single alloy:

- all nine steels (WCB, C5, C12, CA15, CD3MN, CD4MCuN, CF8M, CN3MN, CN7M) can be represented by the benchmark WCB dataset
- Ni-based alloys N3M, CW6MC and CW12MW can be represented by the benchmark CW12MW dataset
- Ni-based alloys M30C and M30-1 can be represented by the benchmark M35-1 dataset

The alloys mentioned above can be grouped in this manner for the *Niyama* simulation qualification casting results. However, caution must be used trying to generalize these groupings to other casting simulation results, because such a generalization neglects important property variation effects.

The effects of property variation on simulation results were studied in the remainder of this work, investigating the variation of (1) solidification shrinkage; (2) liquidus temperature (superheat); (3) solidification path and latent heat; and (4) composition (variations within the specification range). Variations in solidification shrinkage were found to lead to significant differences in riser pipes (both shape and depth), as well as significant differences in the size and severity of porosity indications in the casting. Increasing the superheat was seen to reduce low-Niyama indications, which is interpreted as reducing the amount of solidification shrinkage expected. For a given alloy, significant variations in solidification path and latent heat were seen to have a profound effect on the Niyama results. Finally, variation of composition within the specification range was found to have some effect on the Niyama results, but little effect on the resulting riser pipe prediction. Because the compositional variation in this study ranged from a minimum alloying composition of the specification to a maximum alloying composition, and this variation resulted in only moderate changes in the Niyama contours, one would expect that reasonable variations in chemistry seen in day-to-day foundry practice would have little impact on the Niyama results produced by an accurate dataset for a particular alloy.

A final caution is warranted regarding the idea to use representative datasets for alloys. Done with care, taking into account the points made in this study, reasonable porosity and Niyama results could probably be obtained for many casting simulations. However, the present study only considers Niyama and porosity results, and the Niyama results were only compared with respect to the low-Niyama values used to predict solidification shrinkage. Other results (e.g.,

prediction of hot tears, etc.), or even other uses of the results considered here (such as using higher Niyama criterion values to predict leakers in fluid-containing castings, as discussed in Section 3), could be less accurate if a representative dataset is used.

Acknowledgements

The authors would like to thank Malcolm Blair and Raymond Monroe from the SFSA, for their helpful suggestions and guidance in this work.

References

1. K.D. Carlson and C. Beckermann (2010), "Development of Thermophysical Property Datasets, Benchmark Niyama Results, and A Simulation Qualification Procedure," in Proceedings of the 64th SFSA Technical and Operating Conference, Paper No. 5.5, Steel Founders' Society of America, Chicago, IL.
2. K.D. Carlson and C. Beckermann (2012), "Determination of Solid Fraction-Temperature Relation and Latent Heat Using Full Scale Casting Experiments: Application to Corrosion Resistant Steels and Nickel Based Alloys," Int. J. Cast Metals Research, Vol. 25, pp. 75-92.
3. MAGMAsoft v4.6, Magma GmbH, Aachen, Germany.
4. K. Carlson, S. Ou, R. Hardin and C. Beckermann (2001), "Development of a Methodology to Predict and Prevent Leakers Caused by Microporosity in Steel Castings," in Proceedings of the 55th SFSA Technical and Operating Conference, Paper No. 3.7, Steel Founders' Society of America, Chicago, IL.
5. K.D. Carlson and C. Beckermann (2008), "Use of the Niyama Criterion to Predict Shrinkage-Related Leaks in High-Nickel Steel and Nickel-Based Alloy Castings," in Proceedings of the 62nd SFSA Technical and Operating Conference, Paper No. 5.6, Steel Founders' Society of America, Chicago, IL.
6. S. Ou, K.D. Carlson, R.A. Hardin and C. Beckermann (2002), "Development of New Feeding Distance Rules Using Casting Simulation; Part II: The New Rules," Metall. Mater. Trans. B, Vol. 33B, pp. 741-755.
7. J. Miettinen (1997), “Calculation of Solidification-Related Thermophysical Properties for Steels”, Metall. Trans. B, vol. 28B, pp. 281-297.
8. J. Miettinen and S. Louhenkilpi (1994), “Calculation of Thermophysical Properties in Carbon and Low-Alloyed Steels for Modelling of Solidification Processes”, Metall. Trans. B, vol. 25B, pp. 909-916.

Table 1. Comparison of properties for two WCB alloy datasets.

Alloy	T_{liq} (°C/°F)	Freezing Range (°C/°F)	Latent Heat (kJ/kg)	Solidification Shrink β (%)
WCB-UI	1502 / 2736	91 / 164	180	4.35
C19Mn5	1501 / 2734	39 / 70	274	4.19

Table 2. C12 compositions used to study effects of compositional variation on simulation results.

C12	Elemental Composition (wt %)				
	C	Mn	Si	P	S
Spec.	0.20 max	0.35 - 0.65	1.00 max	0.04 max	0.045 max
Low	0.10	0.35	0.50	0.016	0.007
Actual	0.161	0.460	0.887	0.016	0.007
High	0.20	0.65	1.00	0.016	0.007

C12	Elemental Composition (wt %)				
	Cr	Mo	Ni	Cu	Fe
Spec.	8.0 - 10.0	0.90 - 1.20	0.50 max	0.50 max	bal
Low	8.0	0.90	0.083	0.045	bal
Actual	9.24	1.082	0.083	0.045	bal
High	10.0	1.20	0.083	0.045	bal

Table 3. Comparison of measured liquidus and solidus temperatures with values predicted using IDS.

C12	T_{liq} (°C/°F)	T_{sol} (°C/°F)
Experiment	1492 / 2718	1386 / 2527
IDS	1492 / 2718	1380 / 2516

Table 4. Comparison of liquidus and solidus temperatures and solidification shrinkage among C12 compositions.

C12	T_{liq} (°C/°F)	T_{sol} (°C/°F)	β (%)
Low	1506 / 2743	1439 / 2622	3.94
Actual	1492 / 2718	1380 / 2516	4.29
High	1485 / 2705	1358 / 2476	4.46

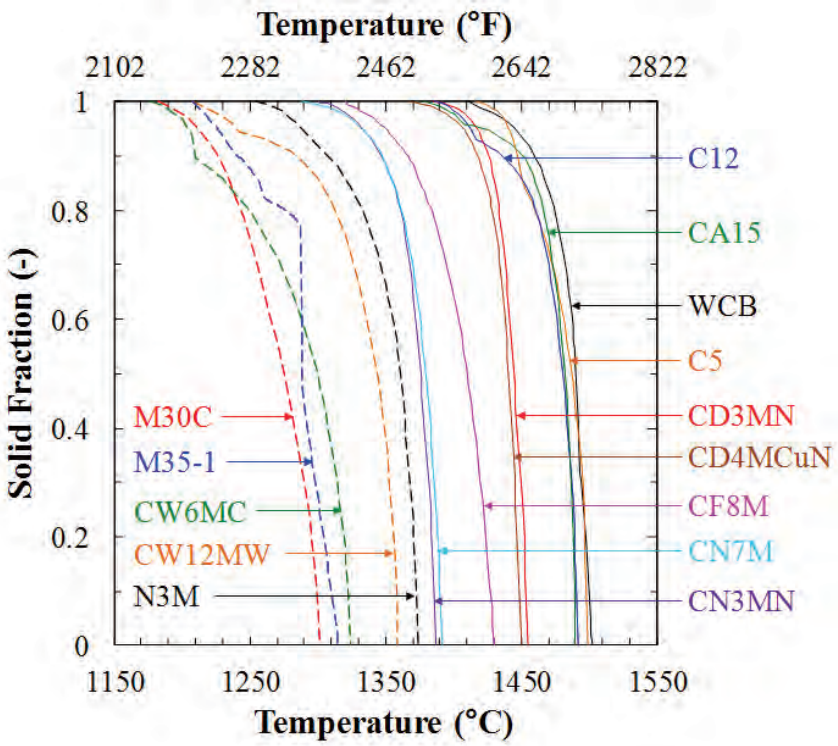

Figure 1. Solidification paths for the 9 steels (solid lines) and 5 Ni-based alloys (dashed lines) currently included in the simulation qualification procedure.

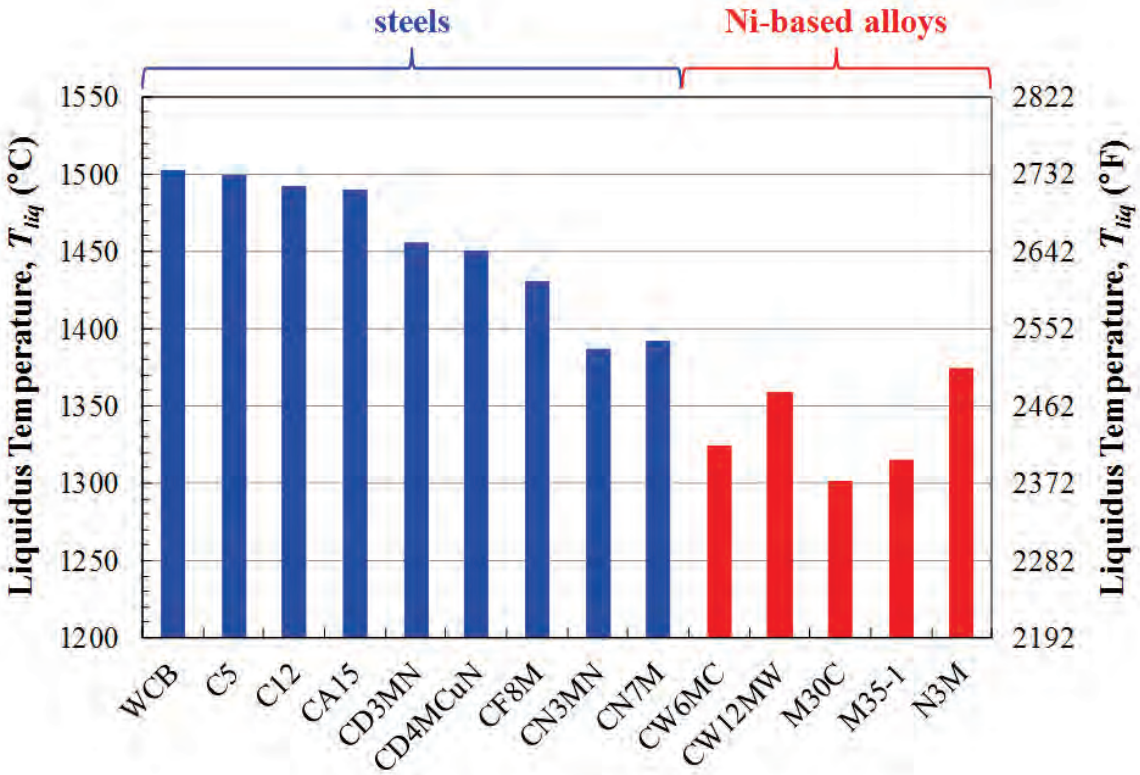

Figure 2. Liquidus temperatures for alloys included in the present study.

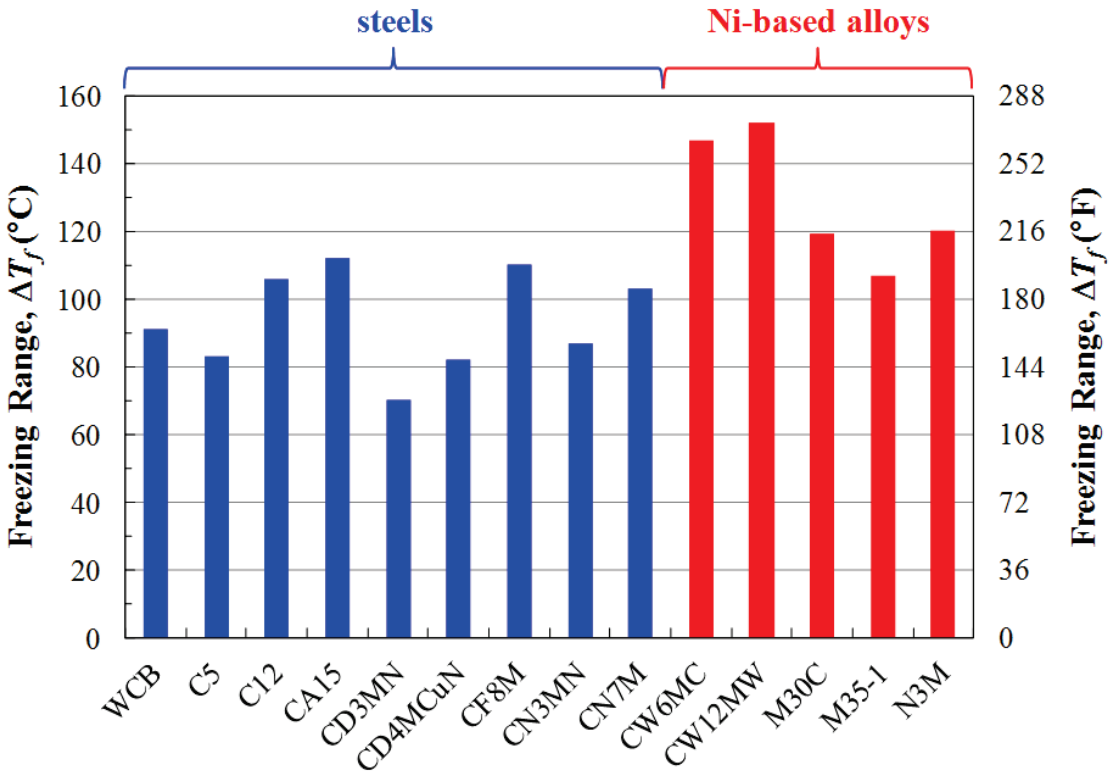

Figure 3. Solidification ranges for alloys included in the present study.

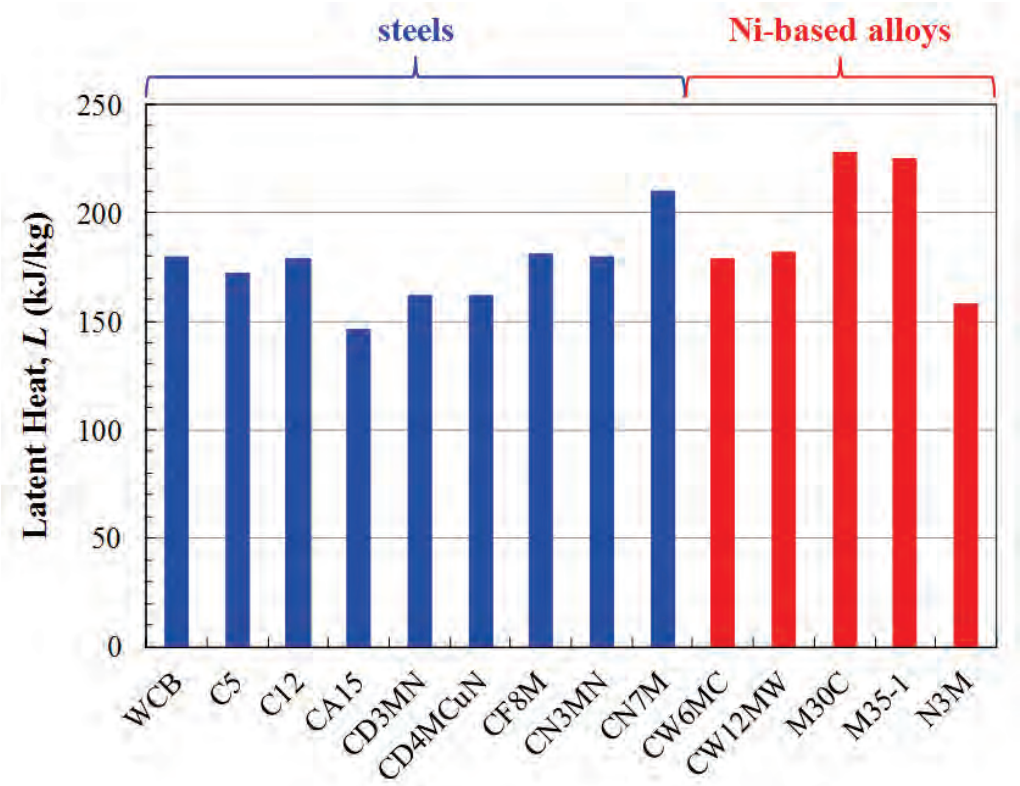

Figure 4. Latent heats of solidification for alloys included in the present study.

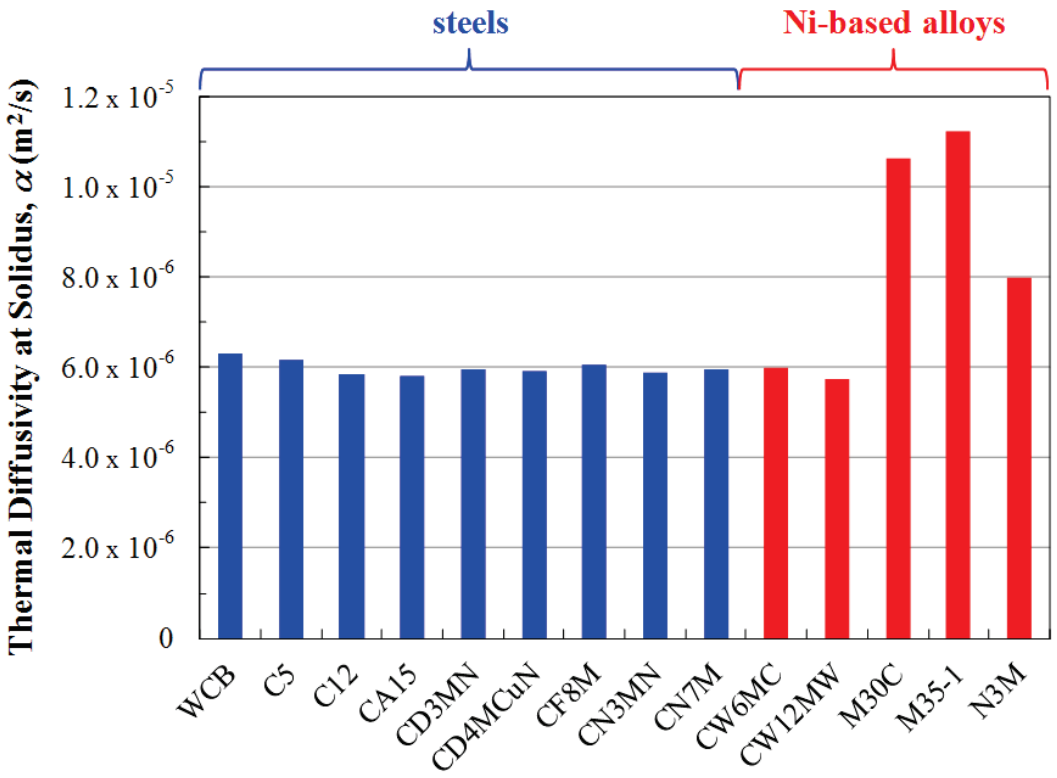

Figure 5. Thermal diffusivity for alloys included in the present study.

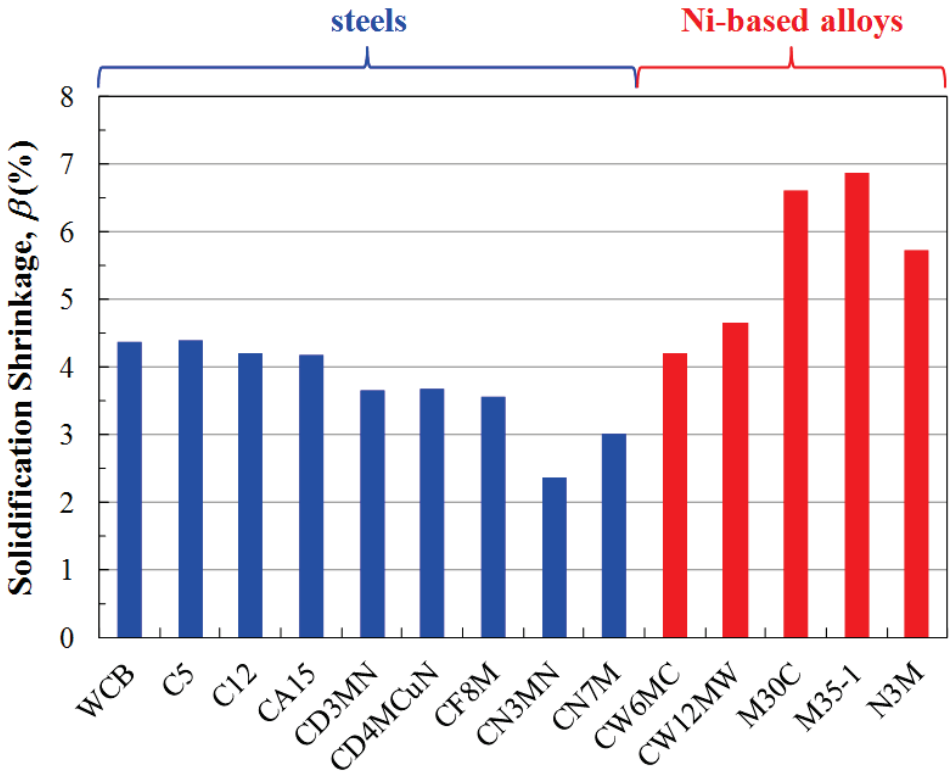

Figure 6. Solidification shrinkage for alloys included in the present study.

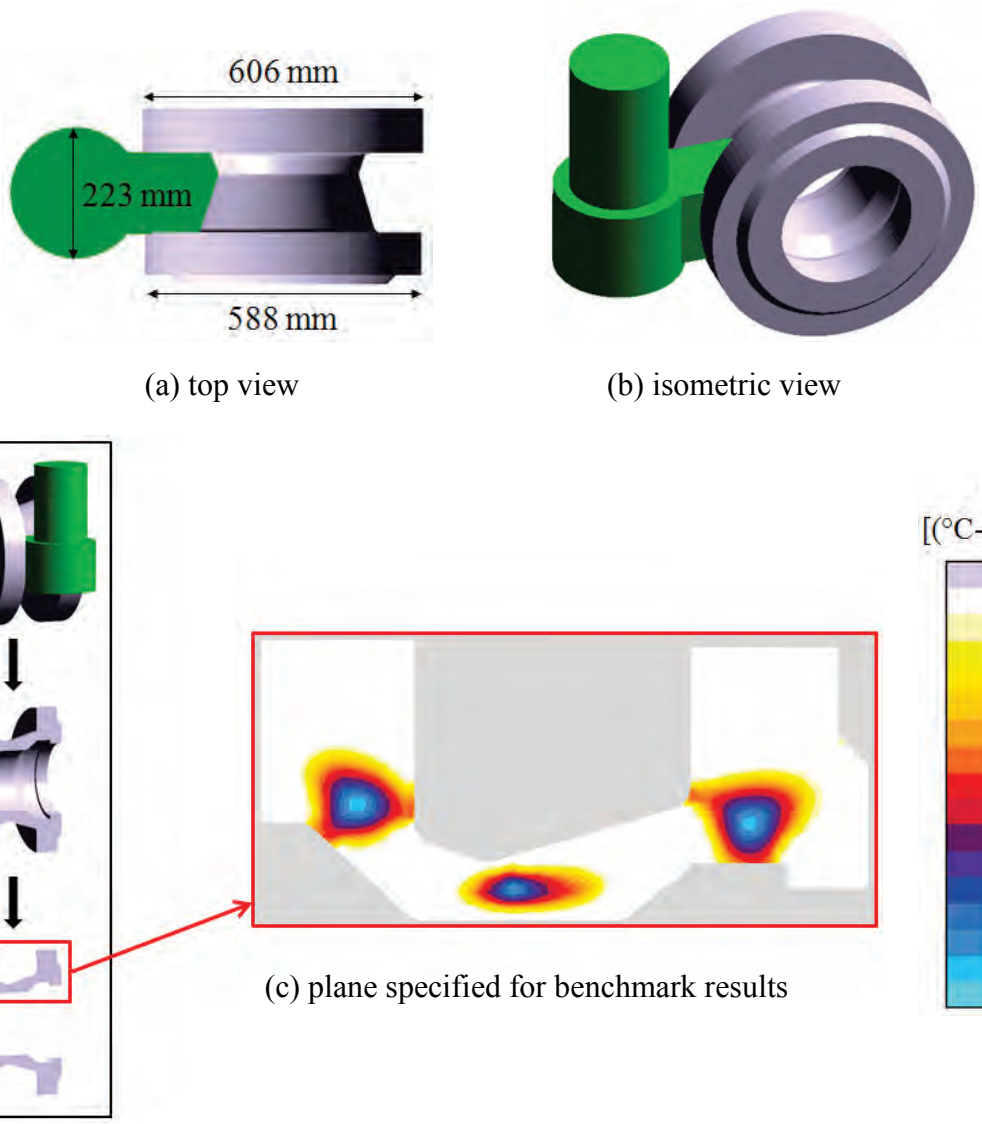

(a) top view (b) isometric view

(c) plane specified for benchmark results

Figure 7. (a) Top view and (b) isometric view of the simulation qualification valve; and (c) plane specified for benchmark Niyama results.

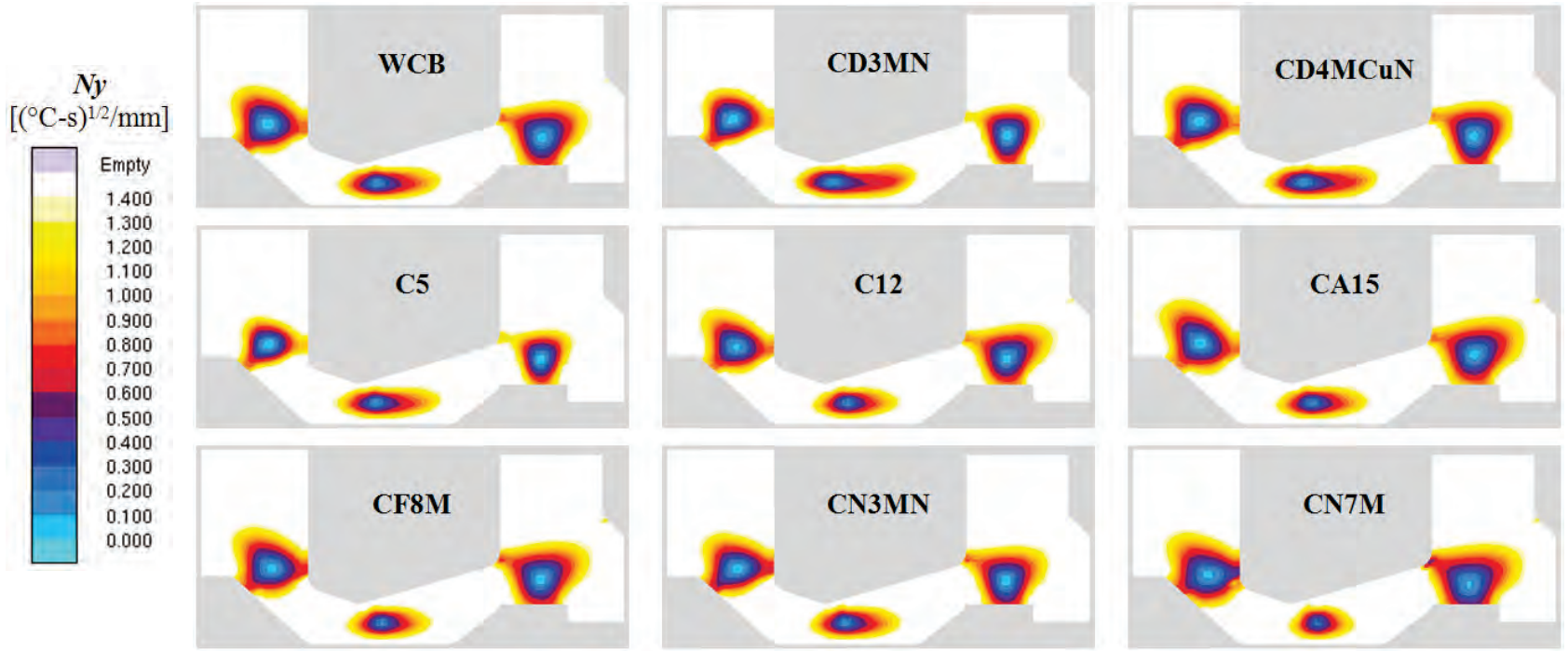

Figure 8. Niyama results for benchmark steel alloys.

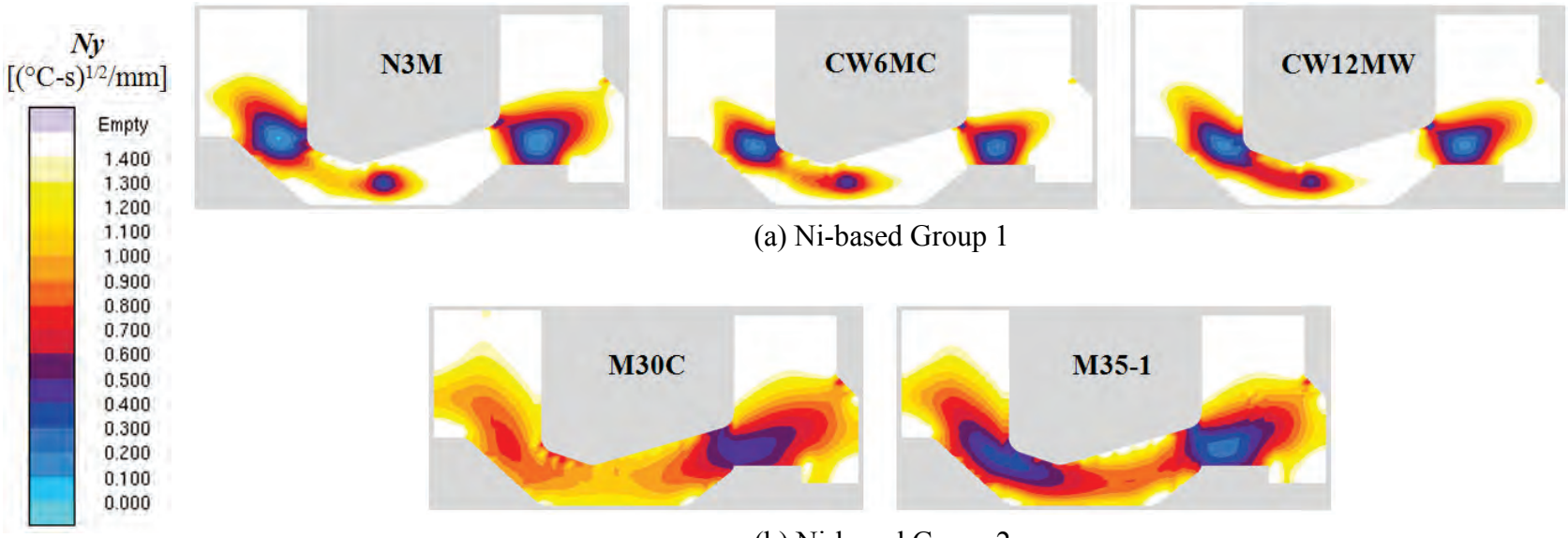

(a) Ni-based Group 1

(b) Ni-based Group 2

Figure 9. Niyama results for benchmark nickel-based alloys.

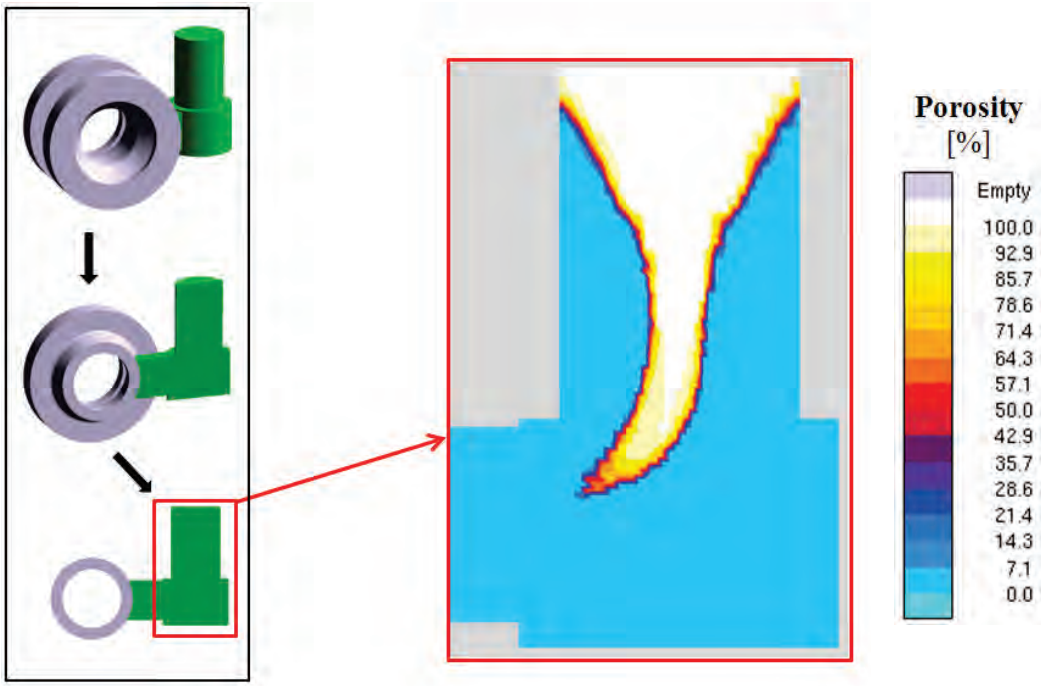

Figure 10. View of simulation qualification valve for riser pipe results.

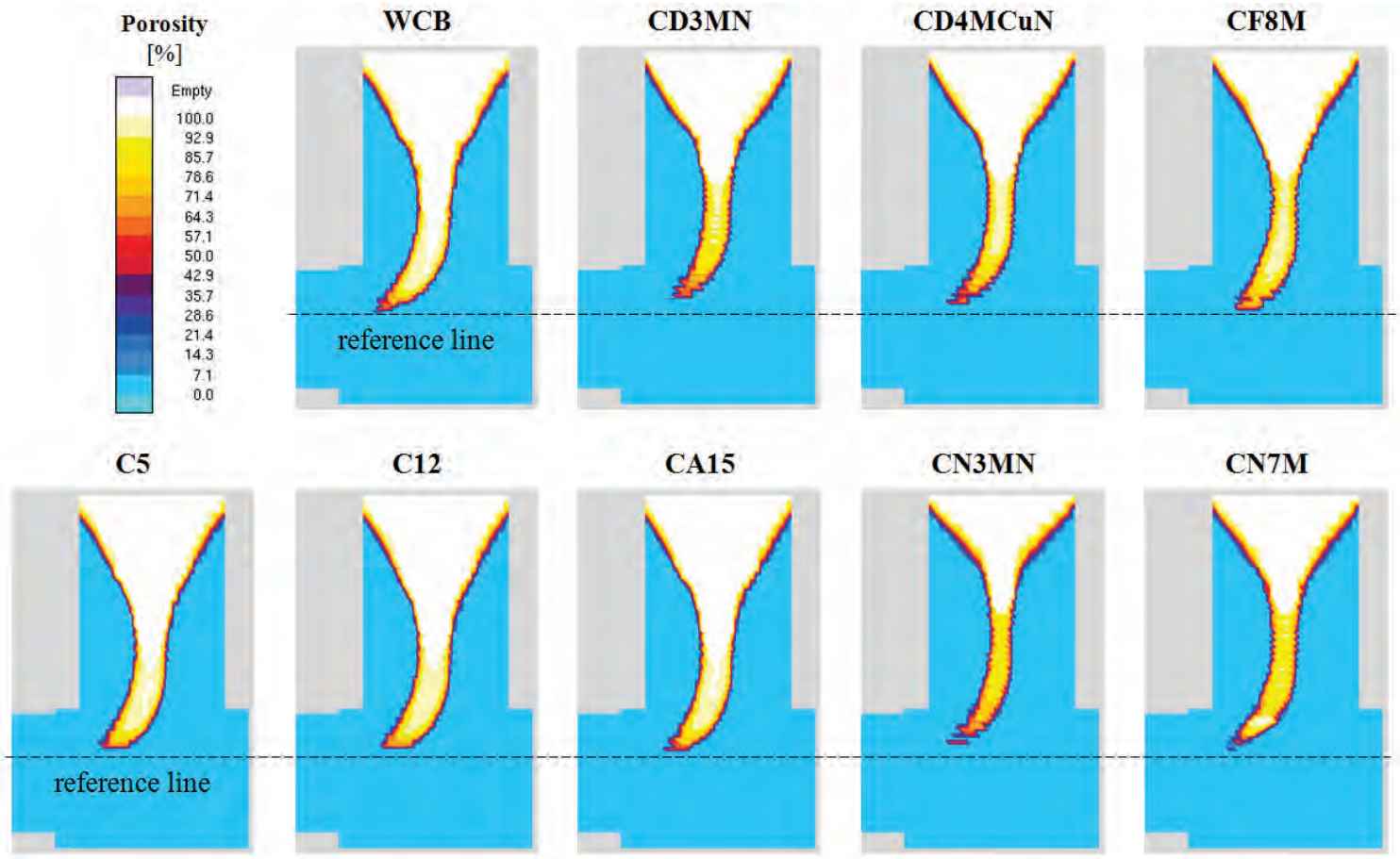

Figure 11. Riser pipe results for benchmark steel alloys.

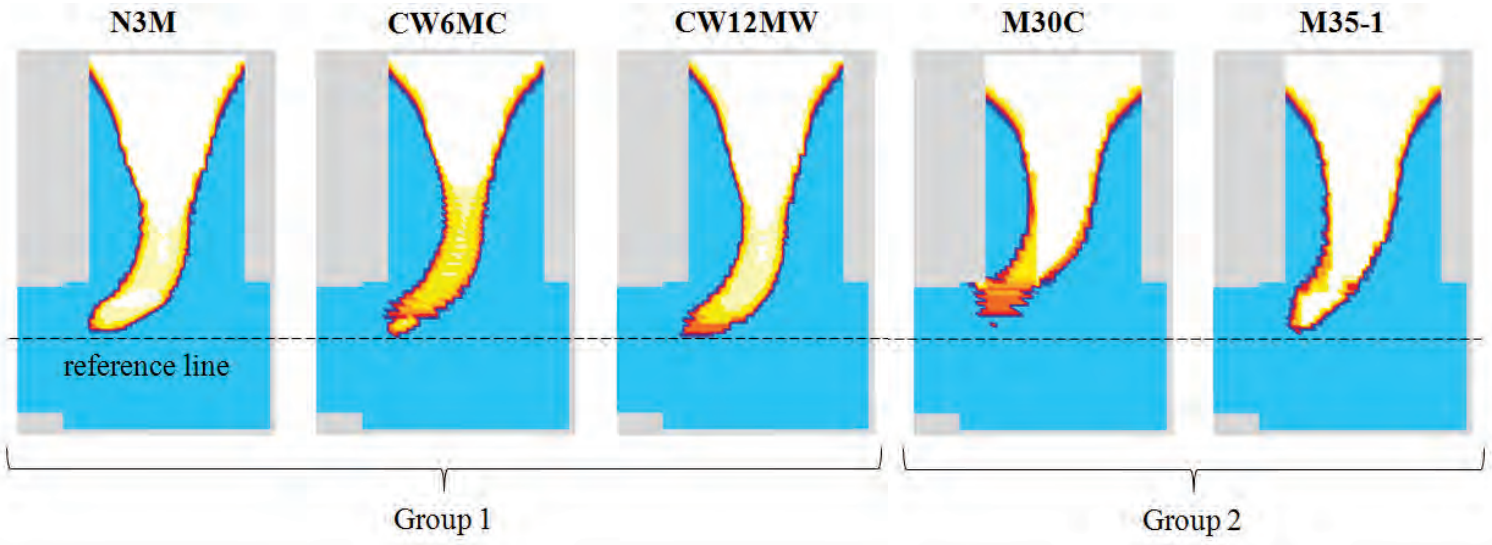

Figure 12. Riser pipe results for benchmark nickel-based alloys. Porosity scale is the same as in Fig. 11.

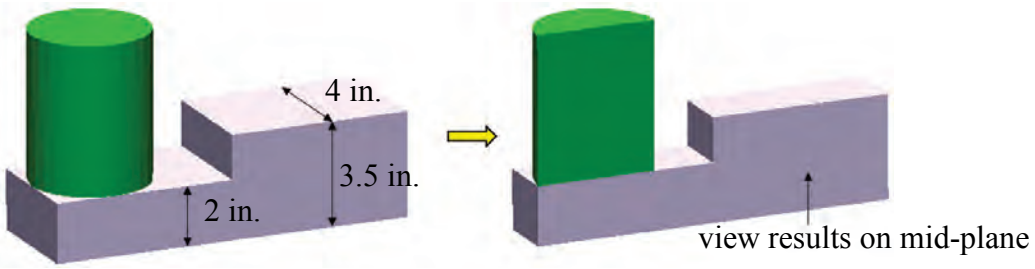

(a) schematic of end-block casting

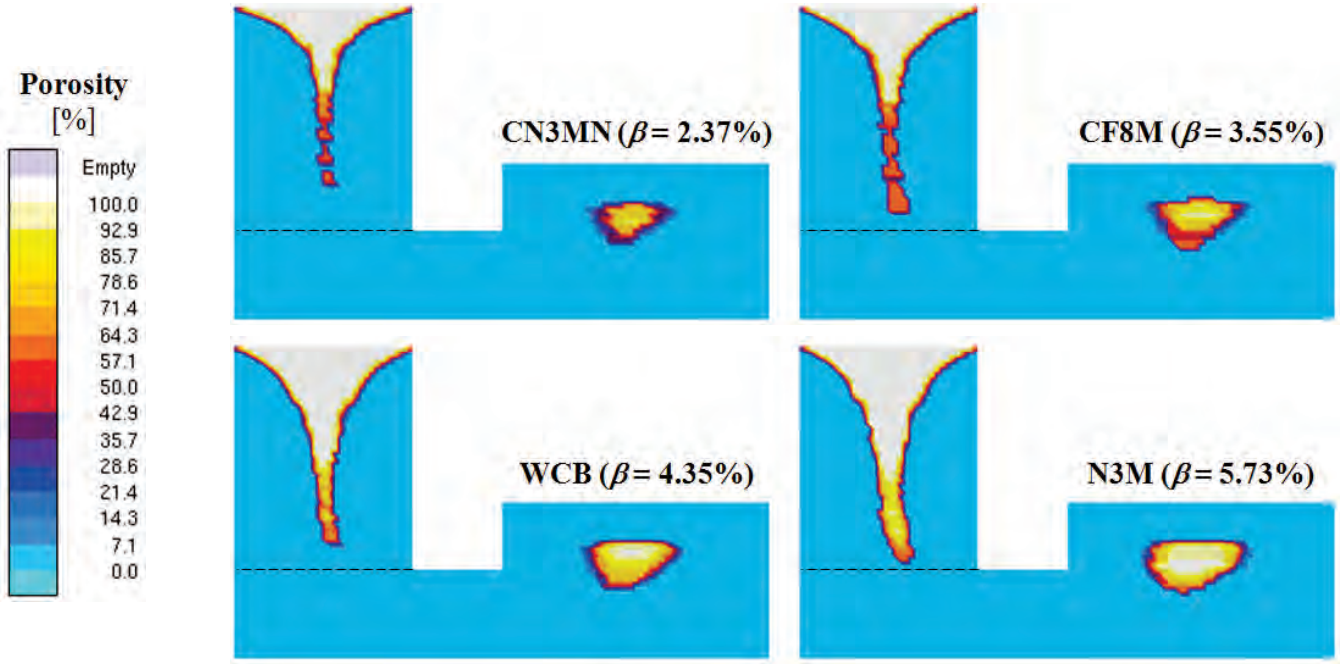

(b) porosity results

Figure 13. (a) Schematic of end-block casting, and (b) comparison of porosity results at casting mid-plane.

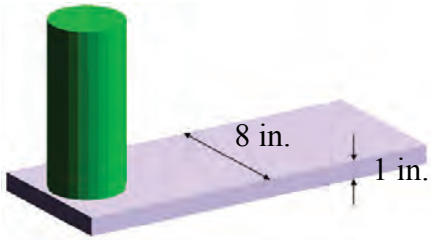

(a) schematic showing plate casting

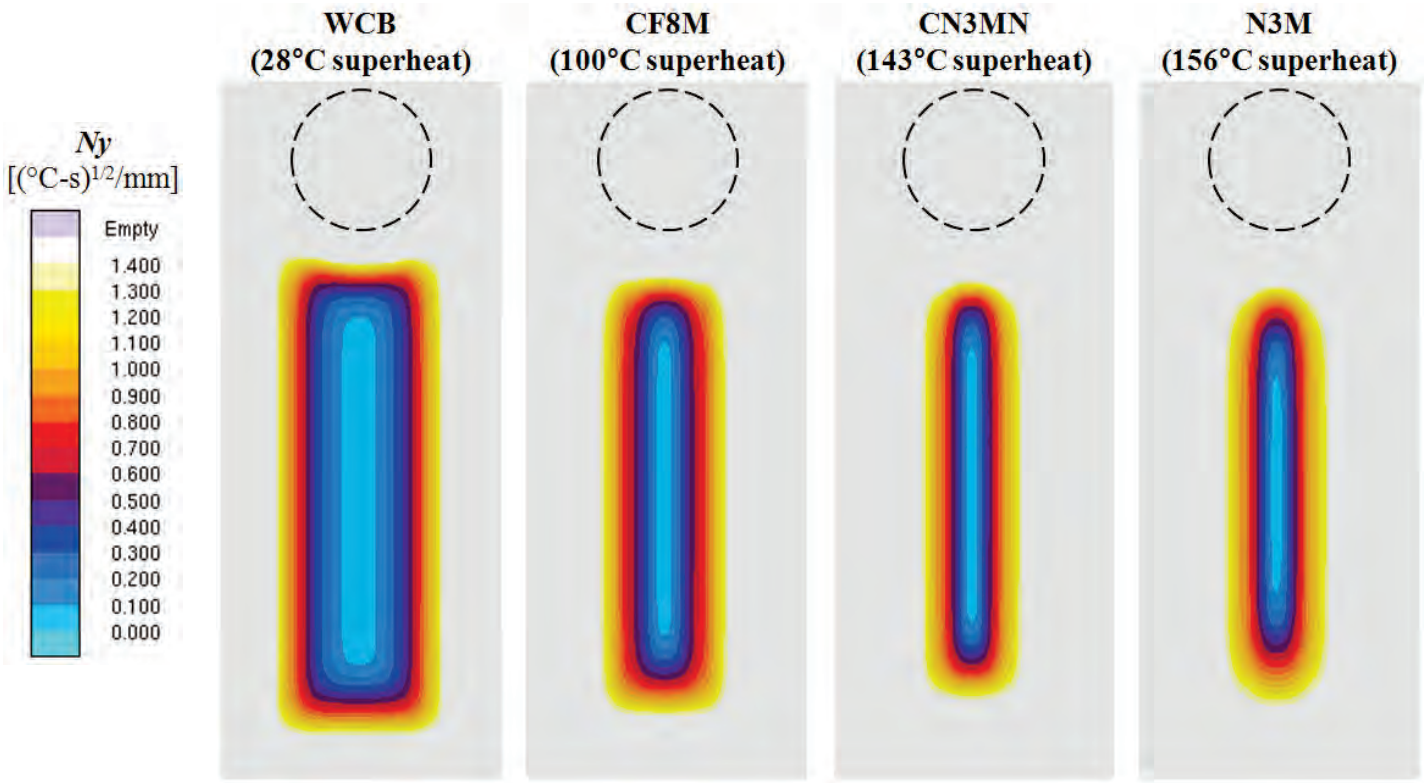

(b) mid-plane Niyama results

Figure 14. Comparison of Niyama results at casting mid-thickness plane for varying liquidus temperatures (superheats).

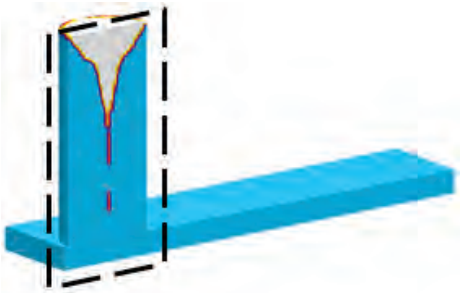

(a) schematic showing riser pipe view

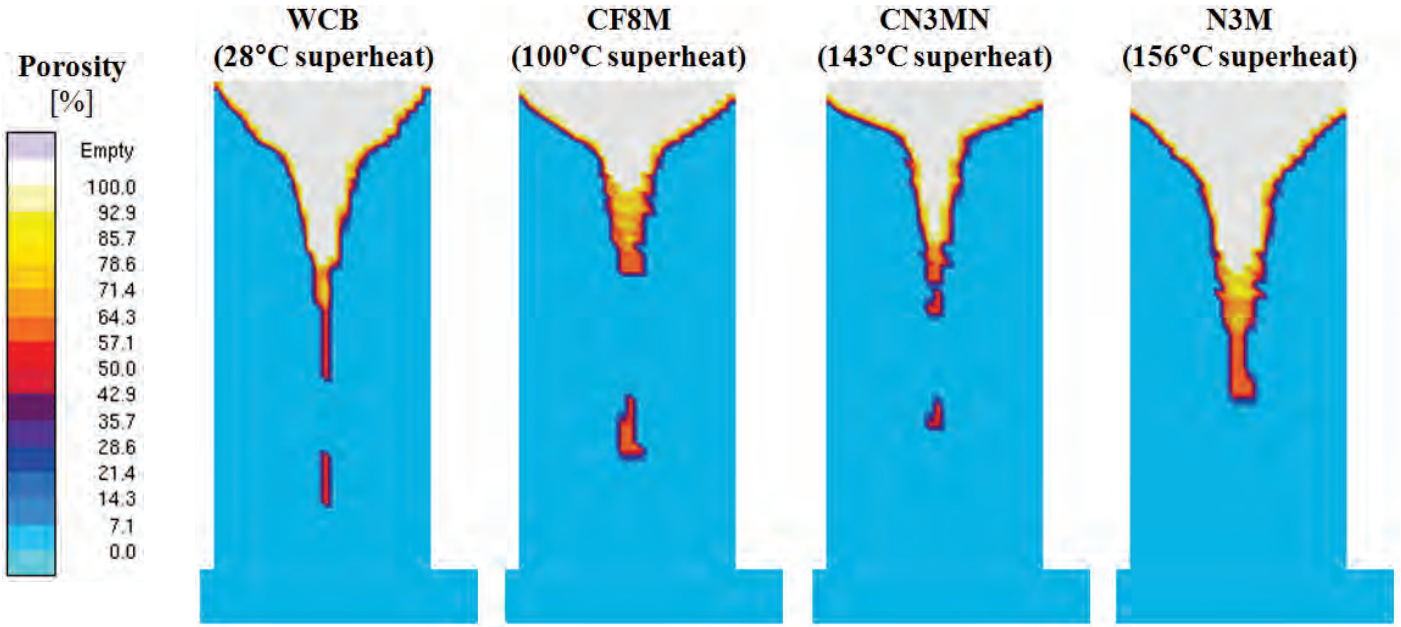

(b) riser pipe results

Figure 15. Comparison of riser pipes for varying liquidus temperatures (superheats).

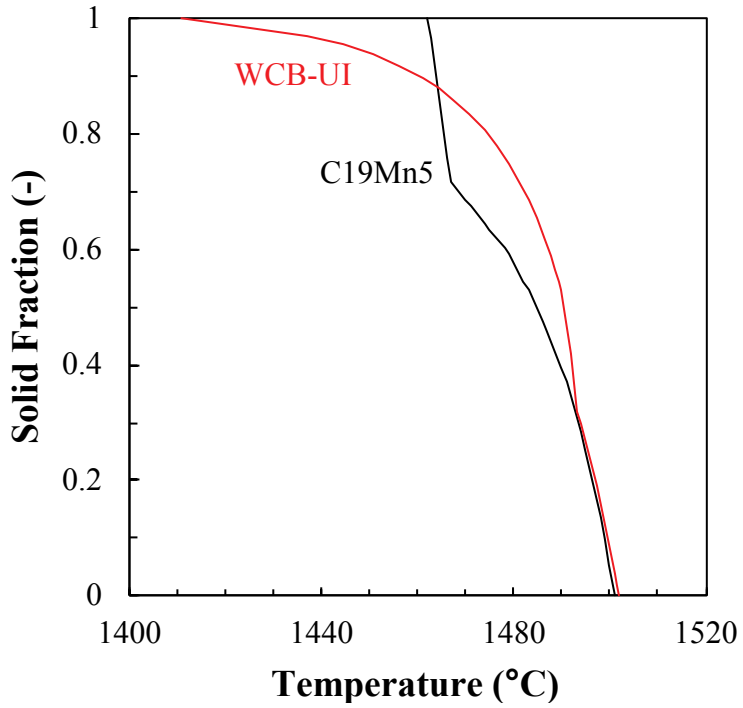

Figure 16. Comparison of solidification paths for two WCB datasets.

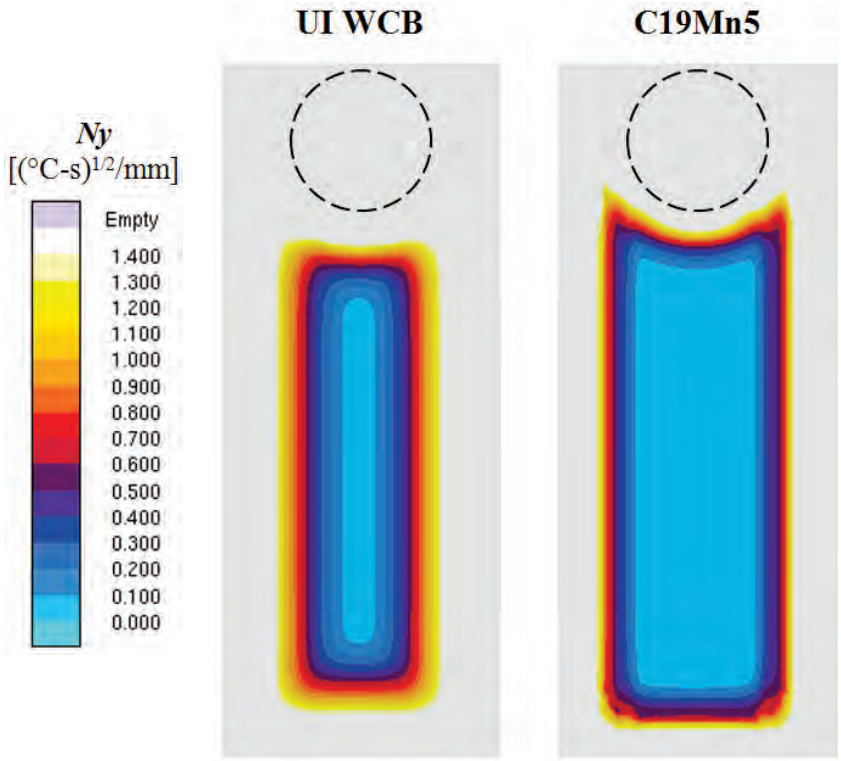

Figure 17. Comparison of Niyama results at casting mid-thickness plane for different WCB datasets.

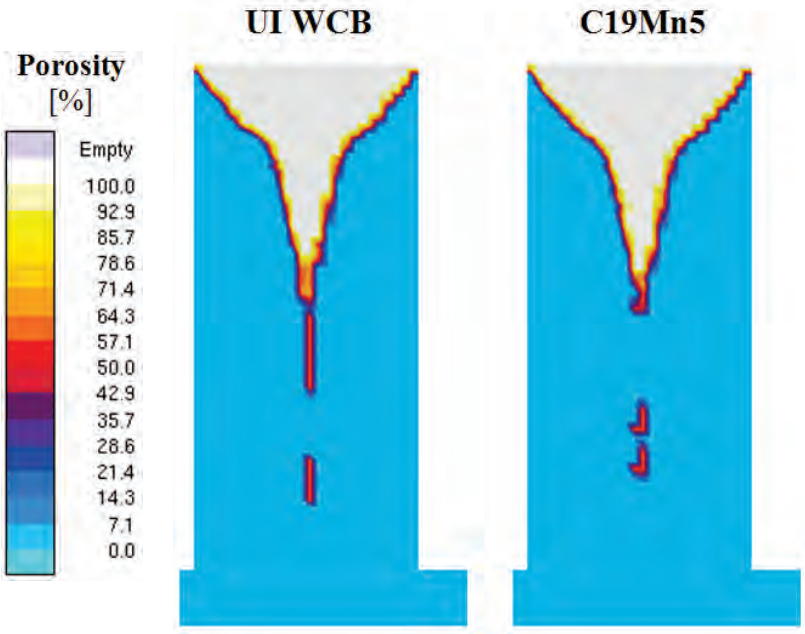

Figure 18. Comparison of riser pipes for different WCB datasets.

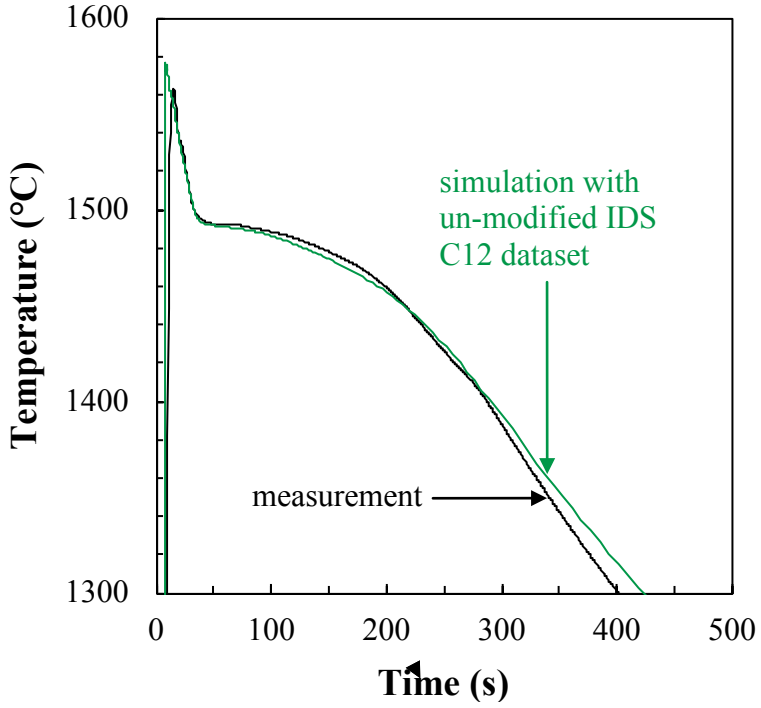

Figure 19. Comparison of measured C12 thermocouple trace and thermocouple trace simulated using un-modified IDS C12 dataset.

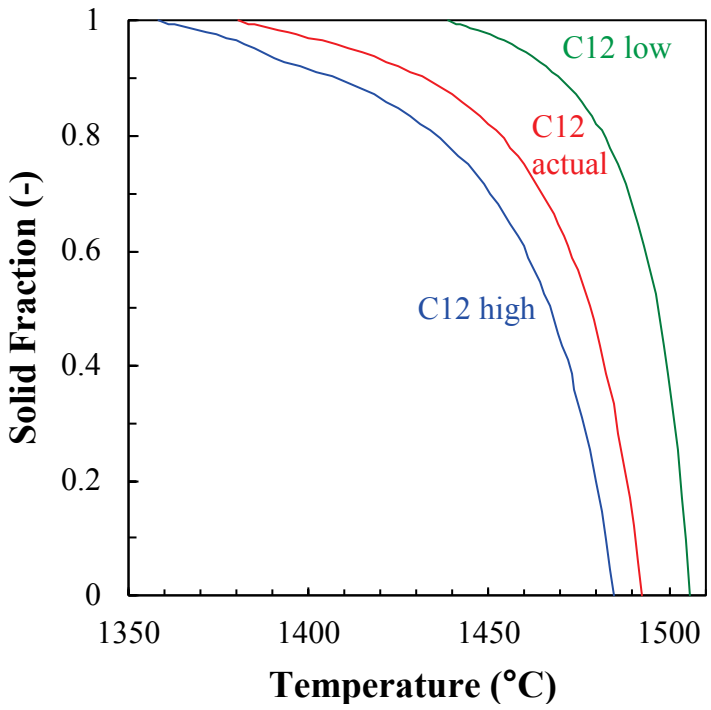

Figure 20. Comparison of solidification paths for different C12 compositions.

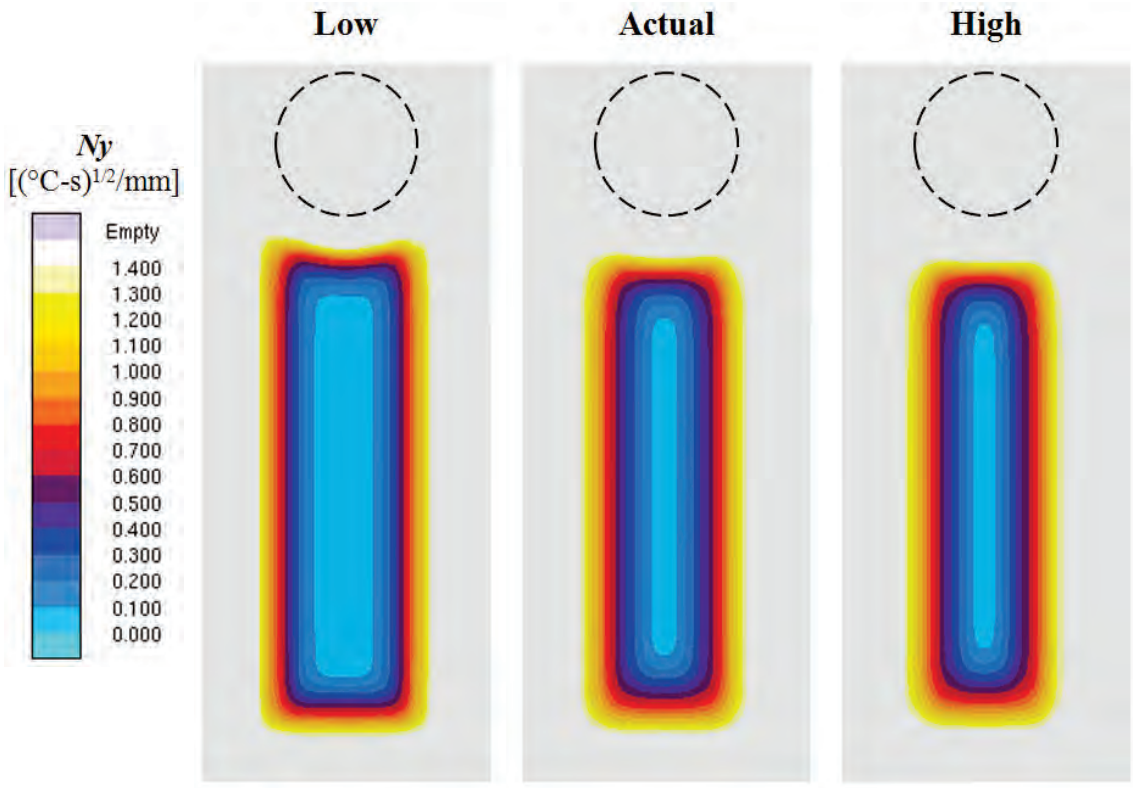

Figure 21. Comparison of Niyama results at casting mid-thickness plane for different C12 compositions.

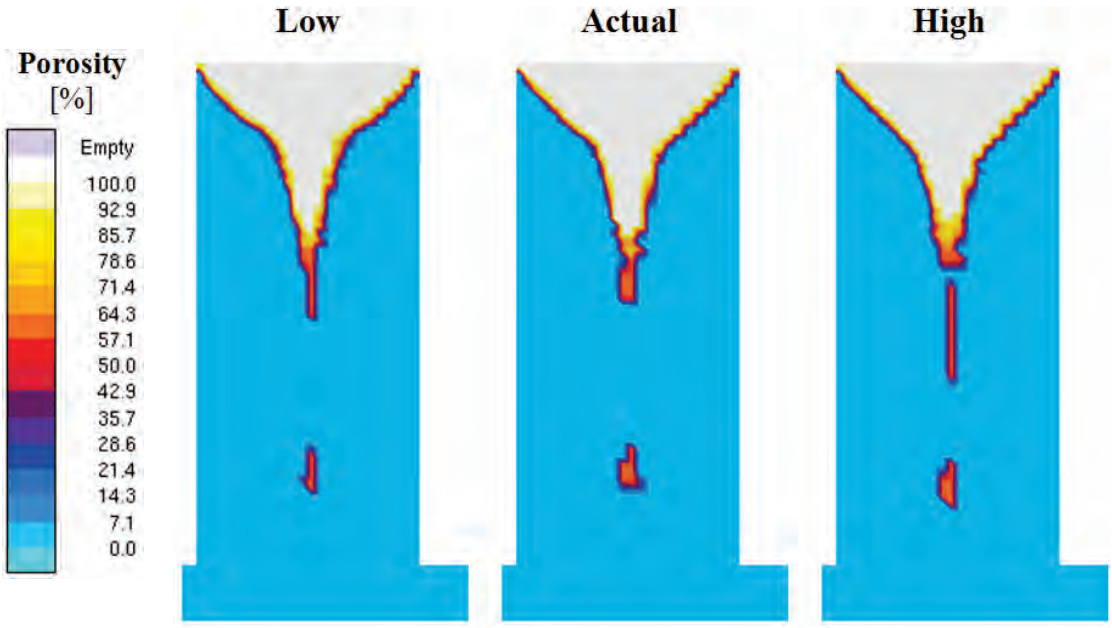

Figure 22. Comparison of riser pipes for different C12 compositions.